Science of the Total Environment xxx (xxxx) xxx

Contents lists available at ScienceDirect

Science of the Total Environment

journal homepage: www.elsevier.com/locate/scitotenv

Identifying a transport mechanism of dust aerosols over South Asia to the Tibetan Plateau: A case study

Tianhe Wang [a], Jingyi Tang [a], Mengxian Sun [a], Xinwei Liu [b], Yuxia Huang [b], Jianping Huang [a,*], Ying Han [a], Yifan Cheng [a], Zhongwei Huang [a], Jiming Li [a]

[a] Key Laboratory for Semi-Arid Climate Change of the Ministry of Education, College of Atmospheric Sciences, Lanzhou University, Lanzhou 730000, China
[b] Lanzhou Central Meteorological Observatory, Lanzhou 730020, China

HIGHLIGHTS

- A typical dust case can affect the Tibetan Plateau (TP) through two routes.
- A secondary circulation triggered by an upper-level jet elevates dust higher.
- High trough and its northward airflows cause the transport of uplifted dust to the TP.
- The evolution of a dust event described by MERRA-2 is consistent with observations.

GRAPHICAL ABSTRACT

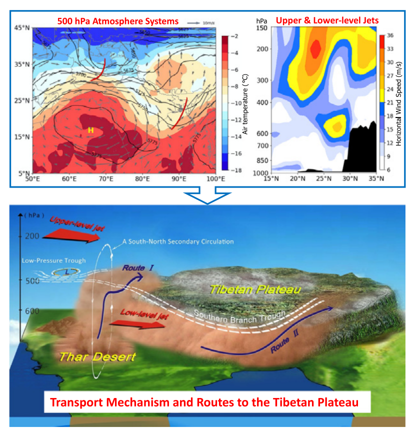

ARTICLE INFO

Article history:
Received 26 August 2020
Received in revised form 9 November 2020
Accepted 9 November 2020
Available online xxxx

Editor: Fang Wang

Keywords:
Dust aerosol
Transport mechanism
Tibetan Plateau
South Asia

ABSTRACT

Dust aerosol, one of the important light-absorbing impurities in snow and ice sheets in the Tibet Plateau (TP), can significantly affect the magnitude and timing of snow melting and glacier recession by altering the surface albedo. It is thus of great importance to understand the potential source and transport mechanism of the dust aerosol over the TP. A typical dust storm case, erupted from the Thar Desert (ThD) in South Asia on 1 to 4 May 2018, was selected to understand synoptic causes and a transport mechanism to the TP using the latest Second Modern-Era Retrospective analysis for Research and Applications (MERRA-2) reanalysis data. Comparing with active/passive satellite-based and AERONET-based observations, the MERRA-2 data provide both the spatio-temporal distribution and evolution process of the dust aerosol more accurately. This study also found that the entire Indian-Gangetic Plain (IGP), Southern India, the Bay of Bengal, and even the TP were influenced by the dust event. The synoptic analysis showed that the dust storm was caused jointly by an upper-level jet stream (ULJS), an upper trough and the subtropical high. A typical south-north secondary circulation adjacent its exit zone, mainly triggered by the ULJS, promoted much stronger and higher vertical uplift of the dust aerosols over the ThD. Consequently, those uplifted dust particles were easily transported to the TP across the majestic Himalayas by the southerly airflows in front of the low-pressure trough over Afghanistan and the southern branch trough over the Bengal Bay. These results indicate that dust aerosol and anthropogenic pollutions constrained and driven by the typical atmospheric circulation condition from South Asia are likely to be transported to the TP. Therefore, it is necessary to further pay attention to the influence of dust aerosols from South Asia on the weather and climate in the TP and its downstream areas.

* Corresponding author.
E-mail address: hjp@lzu.edu.cn (J. Huang).

https://doi.org/10.1016/j.scitotenv.2020.143714
0048-9697/© 2020 Published by Elsevier B.V.

1. Introduction

The Tibetan Plateau (TP), known as the "third pole" of the world, has affected the Asian monsoon system and Northern Hemispheric climatology mainly due to distinctive geographical and complex terrain features. Especially, the TP has experienced a rapidly accelerated warming phenomenon over the last decades (Huang et al., 2012). Furthermore, the retreat of glaciers and an increase in lake levels and river runoff have also been reported over the last decades (Yao et al., 2019). The main driver of these changes is climate change that is dominantly induced by natural variability and human activity at both regional and global scales. A number of studies have demonstrated that the TP has been exposed to polluted air masses that contain light-absorbing aerosols (e.g., black carbon (BC), organic carbon (OC) and mineral dust) from the local and surrounding areas (Huang et al., 2007; Wang et al., 2020a). These strong light-absorbing particles suspended in the atmosphere (Huang et al., 2020) may contribute to alterations in the radiation balance by direct (Sekiguchi et al., 2003; Che et al., 2019a; Wang et al., 2020b), indirect (Huang et al., 2018; Thompson et al., 2019; Yan and Wang, 2020) and semi-direct effect (Huang et al., 2006). Consequently, the altered radiation balance may cause changes in the thermal structure between the TP and surrounding areas, which subsequently induces alterations in not only weather and climate (Huang et al., 2014; Sun et al., 2017) but also the precipitation and monsoon-onset in India (Lau et al., 2006; Meehl et al., 2008). Furthermore, the light-absorbing aerosols deposited onto glacier ice and snowpack may promote their melting, which causes substantial changes in the cryosphere by greatly reducing the albedo of snow and ice (Nair et al., 2013; Li et al., 2017; Gul et al., 2018; Kang et al., 2019). Zhang et al. (2017b) found that BC and dust lying on glaciers in the southeastern TP can reduce the albedo by approximately 20% compared with that of clean snow. Furthermore, they caused the radiative forcing of 1.0– 141 and 1.5– 120 W m^{-2} based on the SNow ICe Aerosol Radiative model (SNICAR). Therefore, identifying the sources and transport mechanisms of the light-absorbing aerosol over the TP is crucial for understanding their effects on weather and climate over the TP (Mao et al., 2019; Hu et al., 2020).

Along with carbonaceous aerosol, dust aerosols, one of the important light-absorbing impurities, have also been observed in snow and glacier sampling in the TP and surrounding areas (Ming et al., 2009; Li et al., 2016a; Li et al., 2016b). It indicates that these impurities are closely related to dust sources, biomass burning and human activities in adjacent areas (Cong et al., 2015; Luthi et al., 2015; Kattel and Yao, 2018). For example, the Cloud-Aerosol Lidar and Infrared Pathfinder Satellite Observations (CALIPSO) satellite confidently detected that dust aerosols accumulated in the Taklimakan desert can be lifted up on the slope of the TP and migrating into the TP (Huang et al., 2007; Luthi et al., 2015; Wang et al., 2020a) and even the western Pacific Ocean (Huang et al., 2008). Furthermore, dust particles in the Northeastern Africa and the Middle East are also transported eastward following the westerly jet and then transported into the TP (Mao et al., 2019; Hu et al., 2020). In this context, the TP plays an important role in the transport features of dust aerosols at a global scale through dynamical and thermal forcing in the mid-latitude (Xu et al., 2018). Remote sensing data demonstrate that dust originated from the Thar Desert (ThD) can be not only frequently accumulated on the southern slope in the TP but also sometimes elevated above 4 km (Ginoux et al., 2012; Tiwari et al., 2019). Moreover, the peak center of dust aerosol optical depth (AOD) tends to move westward and northward during spring (March to May, MAM) to summer (June to August, JJA) along with the onset and intensification of the South Asian Monsoon (Wang et al., 2020b). This means that dust particles suspended in these areas have the potentials to be transported to the TP. Many studies have paid attention to examining the effects of dust particles on Indian monsoon, climate, hydrological system, and radiative forcing over recent years (Vinoj et al., 2014; Pandey et al., 2017; Kaskaoutis et al., 2018). However, few studies have focused on the evolution of dust storm transported from the ThD to the TP.

The selection of the most suitable data is a crucial step to analyze the above evolution of the dust storm. As polar-orbiting satellites usually observe once a day, it is difficult to detect the dust transport process and changes in detail. A model can be employed to produce hourly data that inevitably include high levels of uncertainty in simulations. Alternatively, reanalysis data provide useful information at a sub-daily scale (e.g., hourly, 3-h, or 6-h), which can better depict the evolution of dust events and analyze the transport mechanism. However, it is necessary to comprehensively evaluate the reliability of the reanalysis data to be selected. As the up-to-date Second Modern-Era Retrospective analysis for Research and Applications (MERRA-2) reanalysis data has been recently released and evaluated (Buchard et al., 2017), this study employed the MERRA-2 data to fully explore the potential transport process of a typical dust storm on 1–4 May 2018 over the ThD. The objectives of this study are to (1) fully validate the reliability of spatio-temporal distribution and transport process of the dust storm case depicted by MERRA-2, and (2) enhance our understanding of the plausible transport mechanism of dust aerosol over South Asia to the TP. The paper is organized as follows. Section 2 briefly describes observations and reanalysis datasets used in this study. The spatio-temporal evolution and potential transport of the dust storm retrieved from MERRA-2 are validated with the observations in Sections 3.1 and 3.2, respectively. Section 3.3 comprehensively addresses the synoptic causes and the possible transport mechanism of the typical dust storm case. Finally, the conclusions and discussions are presented in Section 4.

2. Data

2.1. Satellite observations

The Moderate Resolution Imaging Spectroradiometer (MODIS) instrument was launched aboard the Terra and Aqua satellites in 2000 and 2002, respectively. Both Terra and Aqua MODIS instruments play a key role in observing global environmental and climate changes (Savtchenko et al., 2004). They have acquired an extreme volume of data in 36 spectral bands ranging in wavelengths between 0.4 and 14.4 μm for land, atmosphere, ocean and cryosphere since March 2000 for Terra and July 2002 for Aqua. The collection MODIS 6.1 aerosol products are a new "merged" dataset over land and ocean by combining two algorithms: enhanced deep blue over bright surfaces (Hsu et al., 2013) and dark target mainly over vegetated or water surfaces (Levy et al., 2013). This study employed Level 3 daily AOD at 550 nm from Collection 6.1 (MOD08_D3 and MYD08_D3) at a spatial resolution of $1^\circ \times 1^\circ$.

The advanced Ozone Mapping and Profiler Suite (OMPS) currently flying onboard the Suomi NPP spacecraft provide more accurate information to track the current state of the ozone layer with higher fidelity and larger swath than other ozone monitoring systems such as the Solar Backscatter Ultraviolet Radiometer (SBUV/2) and Total Ozone Mapping Spectrometer (TOMS) (Flynn et al., 2009). In addition to monitoring global ozone and other atmospheric parameters related to ozone chemistry and climate, the advanced OMPS can also provide valuable aerosol information (Flynn et al., 2006). The OMPS Nadir-Mapper (NM) instrument measures the ultraviolet (UV) radiance in the range of Huggins bands (300–380 nm) reflected by the Earth's atmosphere and surface, with a 50 km along-track resolution at nadir and a 2800 km wide swath. The UV aerosol index (UVAI), calculated from the radiance residuals in 360 nm, has been actively used to identify and track long-range transport of light-absorbing aerosols in the Earth's atmosphere, e.g., volcanic ash from volcanic eruptions, smoke from wildfires or biomass burning events, dust caused by desert dust storms, and surfaces covered by snow/ice.

The CALIPSO satellite, jointly developed by the United States and France, has been designed to fill the gap of observations between the global distribution and nature of aerosols and clouds by providing

532 nm attenuated backscatter that distinguishes dust from other types of aerosol depending on its capability of depolarization measurements (Winker et al., 2009; Cesana et al., 2016). The CALIPSO-based measurements for aerosol backscatter, extinction and types at a global scale provide essential data to understand dust aerosol features such as the frequency of occurrence (Liu et al., 2008), the transport path (Huang et al., 2015), the dominating aerosol types (Wang et al., 2020a), the dust-forced radiative heating (Wang et al., 2020b) and even global particulate mass concentration (Ma et al., 2020).

2.2. Surface-based observations

The Aerosol Robotic Network (AERONET) program is a global observational network of ground-based remote sensing instruments (i.e., sun photometer). As AERONET measures sun and sky radiances at numerous visible and near-infrared wavelengths, various atmospheric aerosol properties can be provided. In particular, the quality-assured (accuracy less than $\pm$0.01) and cloud-screened Level 2 AOD play an important role in not only understanding global aerosol optical characteristics but also validating satellite retrievals (Holben et al., 1998). The typical dust storm occurred on 1–4 May 2018 has swept many western and northern states of India (i.e., Uttar Pradesh, Rajasthan and Punjab in Fig. 1) along with extremely strong wind speed (>100 km/h), which caused catastrophic damages to infrastructures, vegetation and human life in the regions, e.g., hundreds of uprooted trees, toppled houses, blackout by damaged power lines and casualties (Sarkar et al., 2019). Given the transport direction and potential areas influenced by the dust storms, this study selected the hourly AOD at six stations as shown in Fig. 1 to analyze and validate the evolution of the typical dust storm case depicted by MERRA-2.

2.3. MERRA-2 reanalysis data

The latest MERRA-2 data have been produced from the Goddard Earth Observing System (GEOS) atmospheric model and a cutting-edge data assimilation technique, the Gridpoint Statistical Interpolation analysis (Gelaro et al., 2017). The GEOS model is radiatively coupled with the Goddard Chemistry Aerosol Radiation and Transport (GOCART) model to accurately simulate aerosol-related processes in the atmosphere. Along with conventional meteorological data, the data assimilation has been conducted by bias-corrected AOD derived from the Advanced Very High Resolution Radiometer (AVHRR) over ocean and Collection 5 MODIS products while the AODs derived from Multiangle Imaging Spectroradiometer (MISR) were also employed for data assimilation (Randles et al., 2017). Although MERRA-2 is assimilated with the MODIS and MISR observations, a discrepancy between MERRA-2 AOD versus MODIS AOD of Collection 6.1 has been identified due to inconsistency in AOD collection and retrieval algorithms. This study employed the meteorological fields, the dust column mass density, and the dust aerosol mixing ratio with six different effective radii of MERRA-2 at 0.625° $\times$ 0.5° spatial resolution for understanding the evolution of dust storms and their transport mechanism over the TP.

3. Results

3.1. Spatio-temporal evolution of the dust storm

The dust column mass density (CMD) and total AOD derived from the MERRA-2 reanalysis data were employed to fully understand the spatio-temporal distribution and evolution of the dust storm that occurred in South Asia on 1–4 May 2018 as shown in Fig. 2a and b, respectively. The abundant dust particles, the AOD of 0.7 and dust CMD of

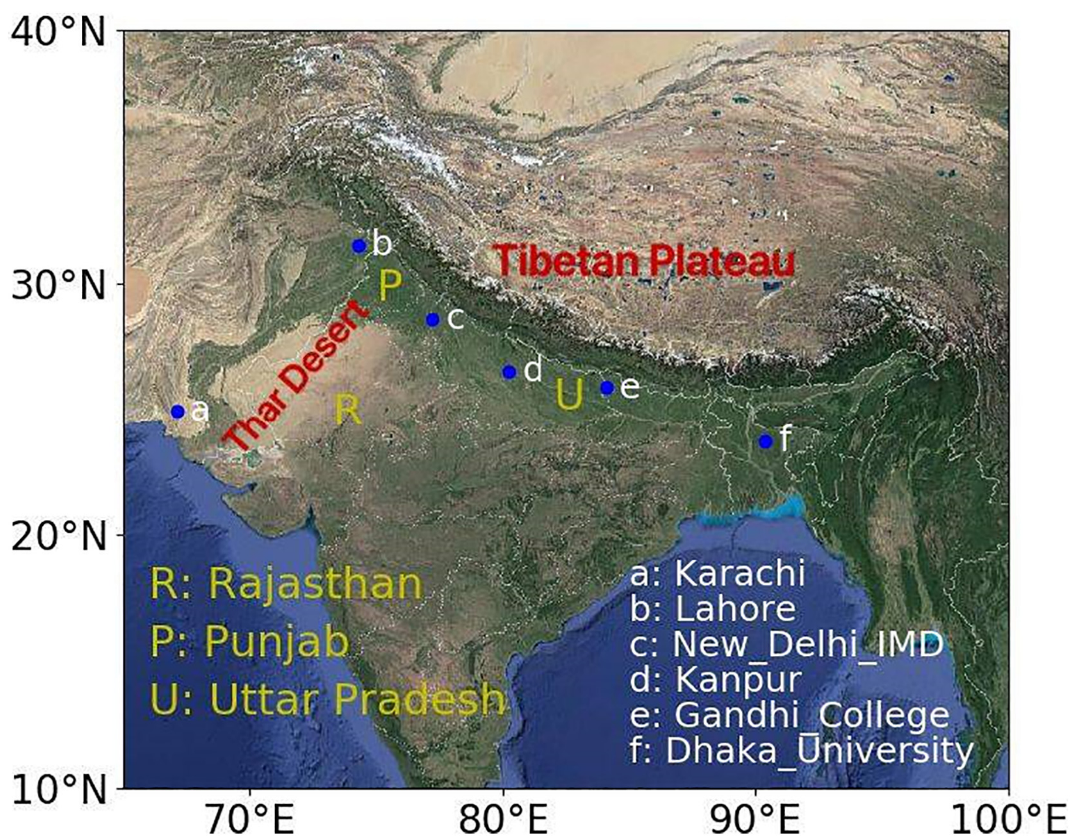

Fig. 1. The surface network of observational stations for dust events and topographical characteristics of TP. The states of Rajasthan (R), Punjab (P) and Uttar Pradesh (U) in India damaged by the dust storm that occurred on 1–4 May 2018 are labeled on the map.

0.8 g/m^2, were mainly concentrated in the ThD on 1 May. Along with the eruption and intensification of the dust storm on the following day (2 May) and incessant emission from the ThD, the peak of AOD and dust CMD in the ThD reached above 1 and 1.8 g/m^2, respectively. Furthermore, the effects of AOD and dust CMD were expanded to adjacent the ThD, i.e., transport and downstream regions. The intensity and impact area of the dust storm began to shrink gradually on 4 May. Given the constraints of local topography and atmospheric circulation conditions, this dust storm accumulated over the Himalayan foothills and traveled eastward and southward (as shown in Fig. 5) and affected the entire Indian-Gangetic Plain (IGP), Southern India, and Bangladesh, which is the most likely phenomenon of aerosol transport over the South Asian during the pre-monsoon (March to May) period. This result is consistent with the previous studies that have investigated the aerosol-related characteristics, transport, and radiative and climatic effect (Gautam et al., 2009; Bucci et al., 2014). A dust plume, with the AOD of 0.5 and the CMD of 0.6 g/m^2, was found over the southern part of Afghanistan and superimposed on the dust released from the ThD during the process of eastward transport. It is also noteworthy that the dust plume directed from southwest to northeast also clearly appeared on the southeast and northwest of the TP (e.g. Fig. 2a-b and d).

However, it is necessary to comprehensively validate whether or not the MERRA-2 data can accurately describe the evolution of the dust event based on other multi-source satellite and surface observations. Fig. 2c and d show the spatial distribution of the dust event observed by the MODIS AOD and the OMPS UVAI. Overall, the spatial distribution of light-absorbing aerosol revealed by OMPS UVAI (>1.0) was consistent with the dust CMD and AOD of MERRA-2 except for spreading over a much wider area. Although MERRA-2 has a greater advantage than the MODIS observations with regard to providing the evolution process of the dust event in detail, there are still significant differences in some regions. Comparing with the MODIS and OMPS observations, MERRA-2 showed a wider spatial distribution of dust aerosols. In the ThD, southern Afghanistan, the Himalayan foothills, and the TP, the peak values of AOD obtained from MERRA-2 were underestimated, ranging from 0.1 to 0.4 on average, while overestimating dust emission from the ThD on 1 and 4 May and dust transport to central India. This discrepancy might be caused by inconsistency in the observations of polar-orbiting satellites between MODIS and the daily average of MERRA-2 reanalysis data. The lack of nitrate aerosols (Buchard et al., 2017) and the underestimation of OC emissions (Randles et al., 2017) in GOCART are necessary to be noted to improve the quality of MERRA-2.

This study also validated the temporal evolution of the MERRA-2 reanalysis data by employing the hourly averaged AODs at AERONET stations. In order to fully cover potential source regions for the typical dust event, this study selected the six AEREONET stations located on the IGP, such as Karachi, Lahore, New_Delhi_IMD, Kanpur, Gandhi_College and Dhaka_University (refer to Fig. 1). Unfortunately, the only QOMS_CAS station in the TP was not included in this study due to the inability to measure data during the period of the dust storm. Fig. 3 shows the temporal evolution of AOD at the six AERONET stations on 1–4 May 2018.

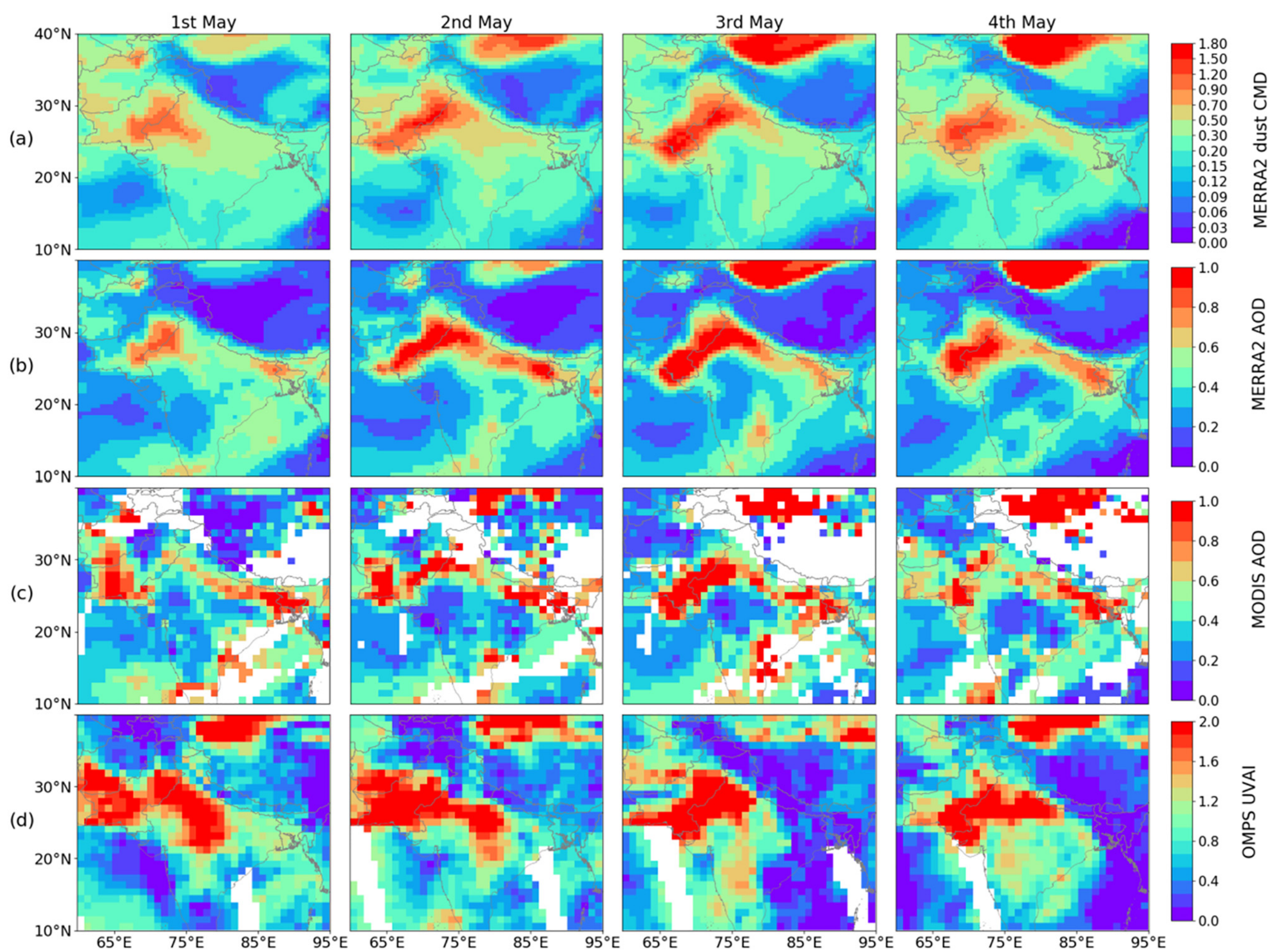

Fig. 2. Spatial distribution of the typical dust storm occurred on 1–4 May 2018 for multi-source datasets: (a) MERRA-2 dust CMD (unit: g/m^2), (b) MERRA-2 AOD, (c) MODIS AOD and (d) OMPS UVAI.

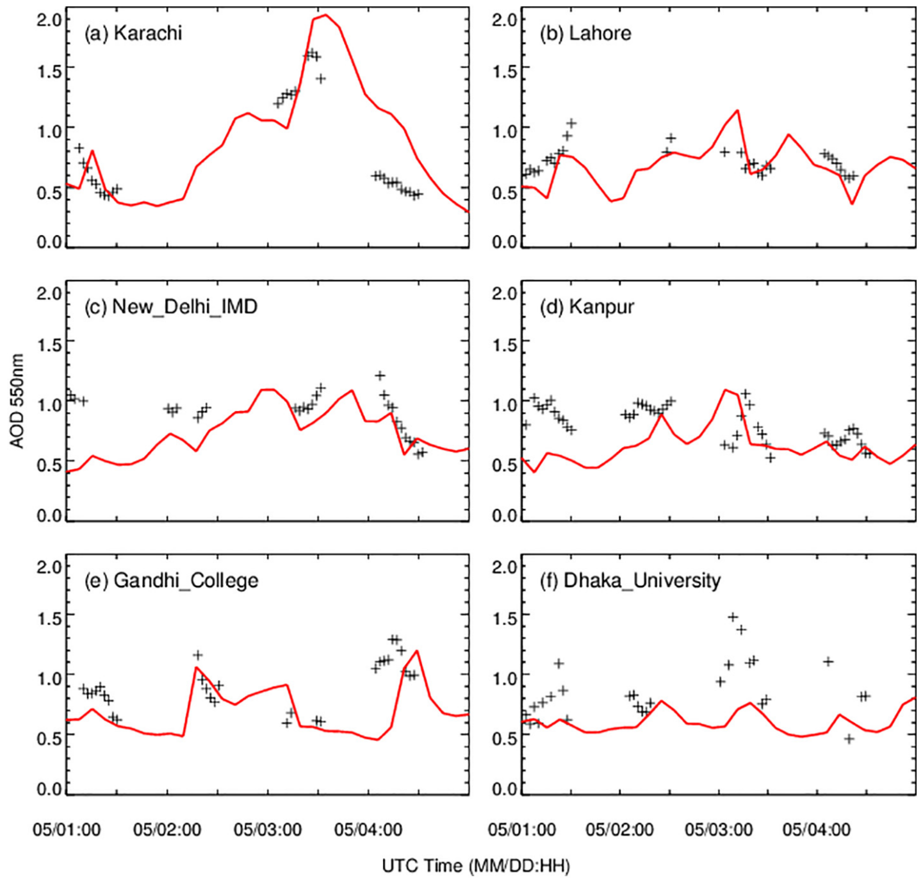

Fig. 3. Temporal evolution of AOD at the six AERONET stations on 1–4 May 2018. The red curve line and the black plus signs represent the hourly averaged AOD for MERRA-2 and AERONET, respectively. (For interpretation of the references to colour in this figure legend, the reader is referred to the web version of this article.)

The results showed that the temporal changes of the MERRA-2 AOD were consistent with those of AERONET over the selected six. The intensity and evolution of dust aerosol released from the ThD can be detected by the change of AOD at the Karachi station close to the ThD (Fig. 3a). The four stations of Lahore, NEW_Delhi_IMD, Kanpur and Gandhi_College were considerably affected by the typical dust storm (Fig. 3b-e). A significant fluctuation of the AOD was observed, which was distributed on 2 May and 3 May. Although the Dhaka_University station was relatively far from the ThD, a similar fluctuation was observed when the dust is transported to the local area. However, the underestimation of MERRA-2 AOD relative to AERONET was evident, i.e., the root-mean-square-error (RMSE) and mean-absolute-error (MAE) are up to 0.25 and 0.20, respectively (Fig. S1). Similar to MODIS, the discrepancy might be mainly attributed to the underestimation of the GOCART model in nitrate aerosols and OC emissions. Overall, the temporal changes of AOD depicted by MERRA-2 at these stations reasonably described the transport direction of the dust from west to east and the spatial distribution based on Fig. 2.

Based on the CALIPSO observations, this study also verified the vertical evolution of the typical dust storm. The strong and deep extinction layers were observed by CALIPSO over the Indian subcontinent and the Bay of Bengal on 2 May 2018 over day and night as shown in Fig. 4. These layers were dominated by dust, polluted dust, or dusty marine depending on locations and the dust particles were uplifted up by 6 km along the CALIPSO tracks, indicating that the dust event affects the Indian subcontinent and the Bay of Bengal. However, the vertical transport of dust aerosol during the daytime might be underestimated due to lower signal-to-noise ratios for the weak extinction layer at higher altitudes, which was caused by the contamination of sunlight. Surprisingly, a thick layer of dust aerosols was also observed by CALIPSO over the southeastern TP on 2 May over the night time, stretching from 4 km to 10 km above sea level, with a maximum extinction of 0.18 km^{-1} near the surface. The potential sources of dust plumes are further discussed in Section 3.2. The dust plume was also well described by the MERRA-2 reanalysis data in Fig. 2.

Overall, the typical dust storm erupted from the ThD over 1–4 May 2018 affected almost the entire IGP, Southern India, and the Bay of Bangle. The spatio-temporal distribution and evolution process described by the MERRA-2 reanalysis data are well consistent with satellite-based and AERONET-based observations. These results demonstrate that the MERRA-2 data can be used to further analyze the potential transmission of dust aerosol to the TP for the dust storm in the following sections.

3.2. Potential transport of dust to the TP

As stated earlier, the deep dust plumes were also observed in the TP during the dust storm investigated in this study. Understanding the transport mechanism relevant to the correlations between the dust storm over South Asia and the dust plume over the TP and is crucial for understanding the potential impacts of this dust process on the TP. This study, therefore, retrieved the dust mixing ratios (DMR) in five size bins and 3D wind fields from the MERRA-2 reanalysis data to examine the above issues. The DMR at different pressure levels was integrated over five size bins to represent the concentration of dust aerosol at this level. To avoid the simulation errors in the MERRA-2 data and to better depict the impacts of dust aerosol on the TP, the anomaly of DMR (ADMR) between the instantaneous one and the background one was calculated in this study. The mean value over March and April 2018 was used as the background of DMR in this study.

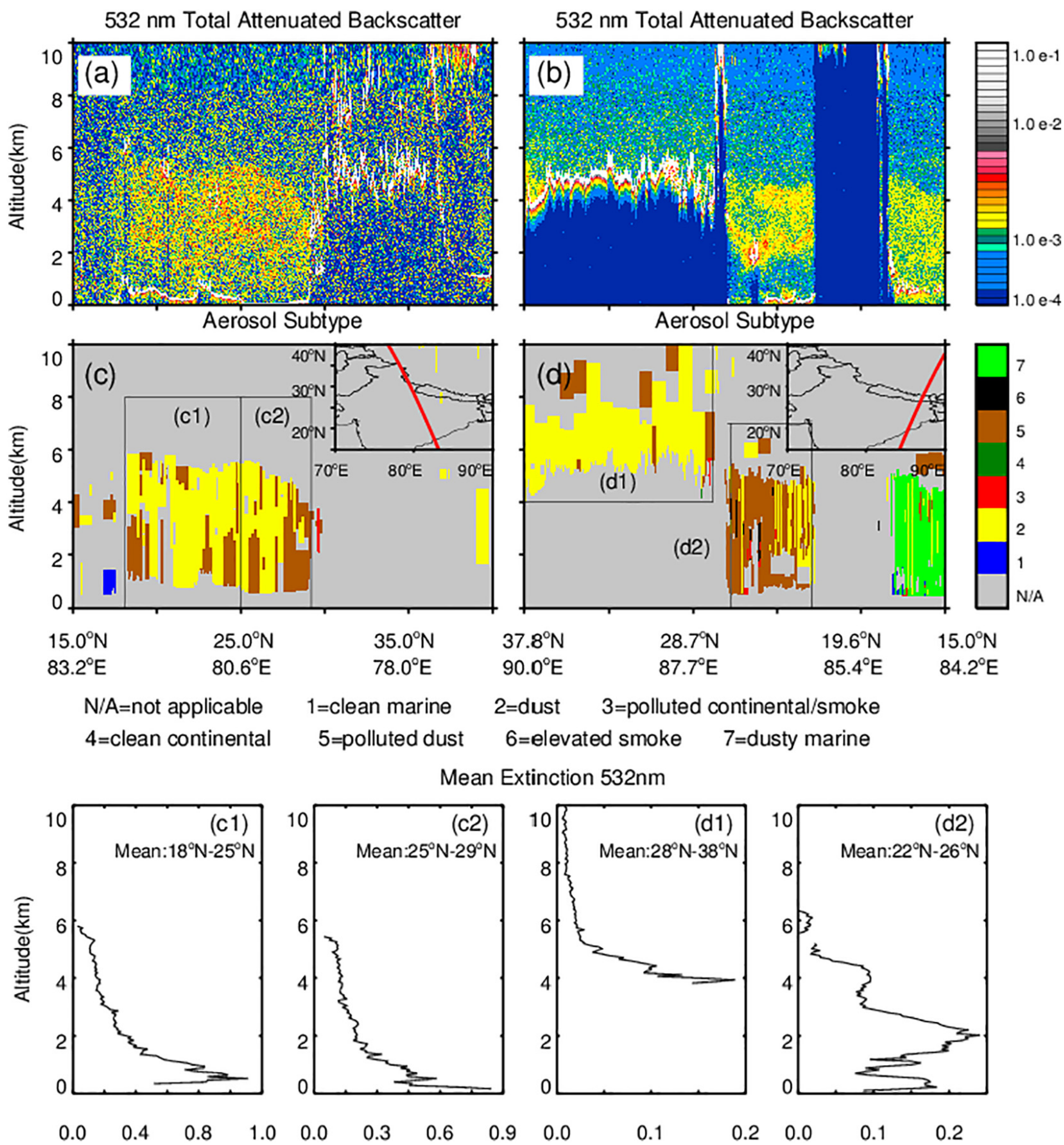

Fig. 4. Vertical distributions of (a, b) 532 nm total attenuated backscatter (km^{-1} sr^{-1}), (c, d) aerosol types, and (c1, c2, d1, d2) 532 nm mean aerosol extinction coefficient (km^{-1}) over four specified areas along the CALIPSO tracks in the morning (left) and evening (right) on 2 May 2018.

In Fig. 5, the horizontal distribution of column-integrated ADMR from 337.5 hPa to 525 hPa is presented to identify the potential transport of the dust aerosol during the dust event at the upper level. The positive peak center of ADMR appeared mainly at the ThD and its adjacent areas, indicating that large amounts of dust aerosols uplifted above 500 hPa are driven by strong upward movements (29°N) as shown in

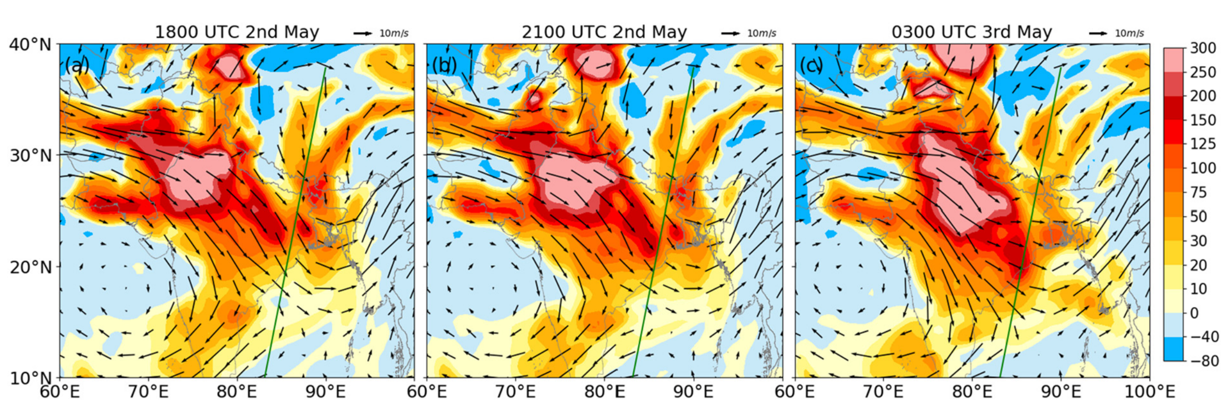

Fig. 5. Horizontal distribution of the column-integrated ADMR (unit: ppbm; shading) from 337.5 hPa to 525 hPa and total wind vectors (unit: m/s; arrows) at 412.5 hPa level at different times. The green line represents the CALIPSO track on 2 May 2018 over the night time. (For interpretation of the references to colour in this figure legend, the reader is referred to the web version of this article.)

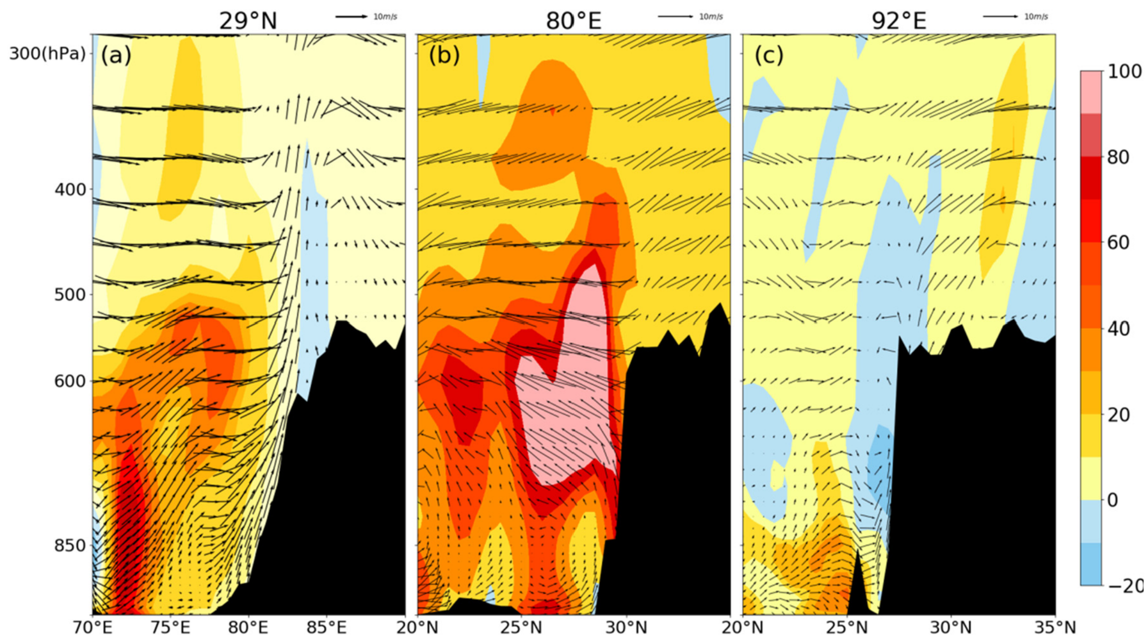

Fig. 6. Vertical cross-sections of the ADMR (unit: ppbm; shading) at (a) 29°N, (b) 80°E, and (c) 92°E. The zonal and meridional circulation (unit: m/s) were superimposed on these images respectively.

Fig. 6a. Given the influence of upper northwest airflows controlled by the subtropical high over the Indian Ocean, the dust aerosols continuously transported from the ThD were mainly affecting the downstream region and even the TP. Significant positive ADMR was found at two typical areas over the TP as shown in Fig. 5. One mainly appeared at the western TP about 80°E, where the dominating wind direction partly shifted from the northwest to the south. Most of the dust aerosols uplifted by strong vertical movement (Fig. 6a-b) were transported to downstream by the dominating northwest wind and consequently, Southern India and the Bay of Bengal were influenced by this dust aerosol transport. On the contrary, the rest was transported to the TP by the enhanced southerly wind, resulting in a larger ADMR and wider areas influenced over the western TP (Fig. 5b-c). The other was found at the southeastern TP in which a cyclonic curved southwest-northeast belt was detected. The dust belt observed by the CALIPSO satellite (Fig. 4d) was extended from the Bay of Bengal to the eastern TP under the primary driver of strong southerly wind, which is consistent with the previous studies that examined the water vapor transport channel to the Yangtze River basin of China (Dong et al., 2019; Yang et al., 2019). The results indicate that dust aerosols and other pollutions over South Asia can be transported across the majestic Himalayas through various routes, resulting in impacts on the weather and climate in the TP and part (the middle and downstream regions) of the Yangtze River.

3.3. Circulation conditions and transport mechanism

The emission and transport of dust are usually dominated by atmospheric circulation and meteorological elements (Che et al., 2019b; Harrison et al., 2019). As shown in Fig. S2, the geopotential height at 500 hPa level showed that the western Indian subcontinent was affected by the subtropical high centered in the Arabian Sea. In addition, a relatively strong southern branch trough (SBT) over the Bay of Bengal was found before the outbreak of this dust storm. Therefore, a cold advection over the ThD was driven by the northwest airflows behind the SBT. Based on the temperature at 850 hPa and sea level, a higher temperature occurred over the entire area of the ThD. In particular, the surface temperature across India at sea level increased significantly on 2 May. Such a vertical temperature profile in the atmosphere is usually caused by the cooling of the upper air and the warming of the lower air, inducing strong convective effective potential energy that causes atmospheric instability. As the low-pressure trough (LPT) at the 500 hPa over northern Afghanistan moved southeastward by the night on 2

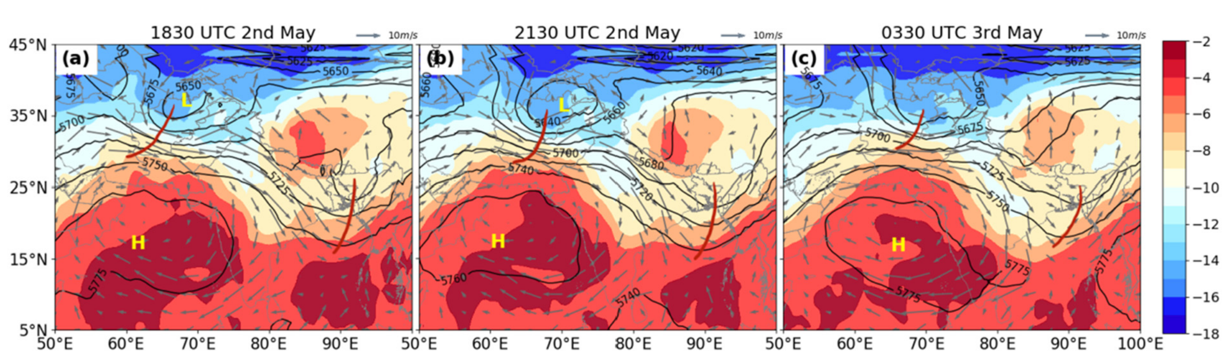

Fig. 7. Composite distribution of air temperature (unit: °C; shading), geopotential height (unit: dagpm; black contours) and total wind vectors (unit: m/s; arrows) at 500 hPa. The red curves represent the trough lines. The centers of subtropical high and low-pressure are labeled as the yellow letter H and L respectively. (For interpretation of the references to colour in this figure legend, the reader is referred to the web version of this article.)

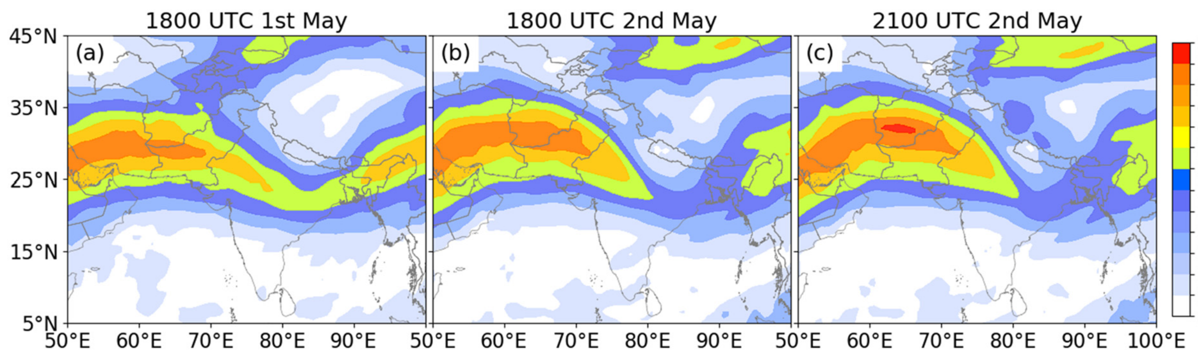

Fig. 8. Horizontal wind speed (unit: m/s) of the ULJS at 200 hPa level.

May, the southward cold air mass in northwestern India caused a further decrease in the temperature of the upper air over the ThD, which eventually triggered strong convective weather that creates momentum to lift the mineral dust in the ThD into the air and eventually forms a severe dust storm.

The southerly airflows at the upper level are a key dynamic factor that transports the uplifted dust aerosols to the TP. Fig. 7 shows the composite weather pattern during the strongest dust storm period from 2 May to 3 May. The cold low-pressure over northern Afghanistan moved southward on 2 May overnight, and the southerly wind component in front of the LPT increased along with enhancing the cold low-pressure. Thereafter, in the early morning on May 3, there was even a southerly wind in the southwestern TP that carries the dust to the TP (Fig. 5c). Besides, the SBT over the Bay of Bengal was another important contributor. The temperature field was westerly more than the geopotential height field, indicating a cold advection

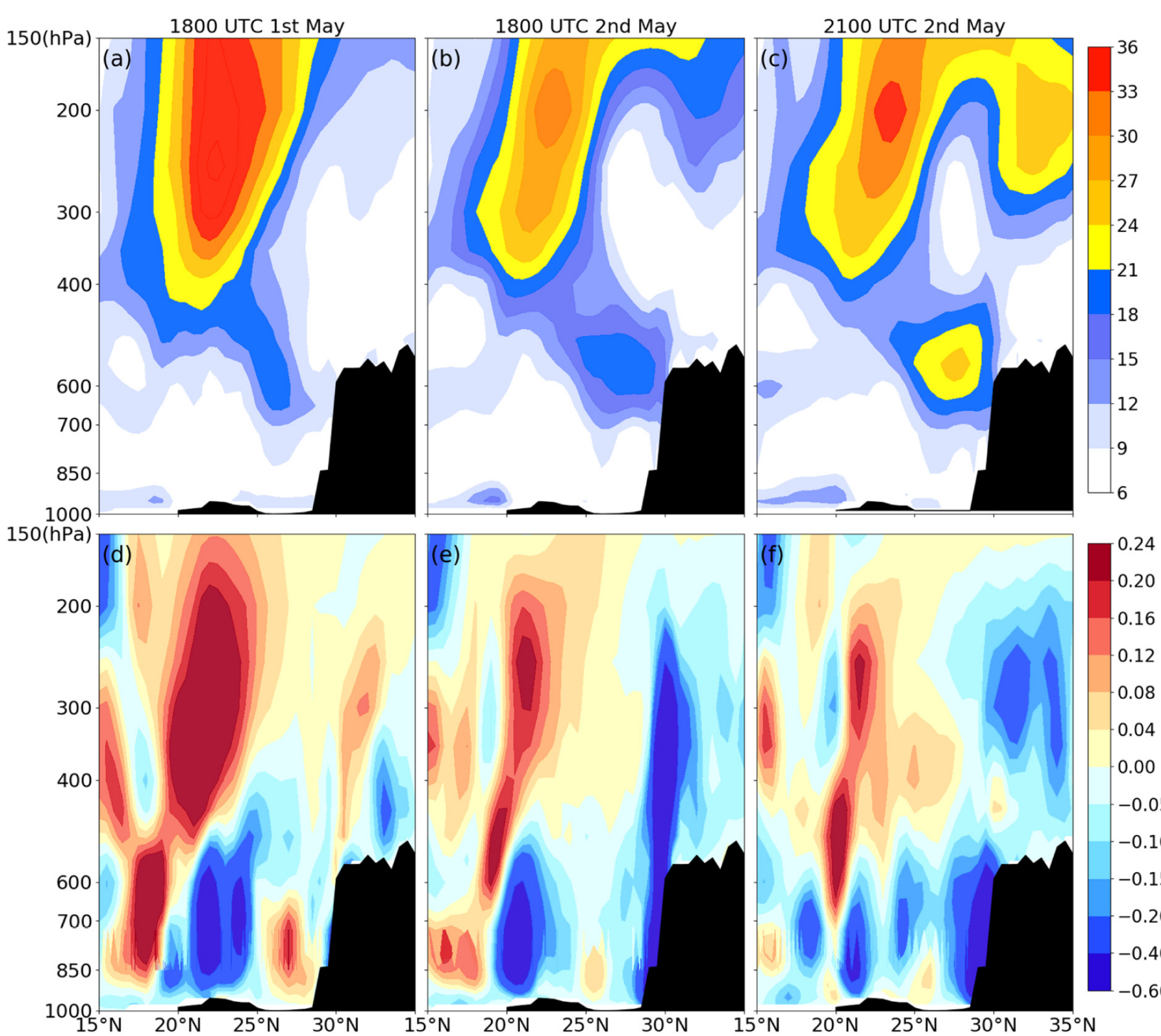

Fig. 9. The vertical cross section of (a-c) horizontal wind speed (unit: m/s) and (d-f) vertical speed (unit: Pa/s) at the exit area of UJLS (80°E).

behind the SBT that promotes the sinking movement and dust deposition. In contrast, a warm advection in front of the SBT was conducive to the upward movement and the uplift of dust. Therefore, the southwest airflows in front of the SBT can eventually transport dust aerosols to the TP.

Besides, heavier dust storms accompany the upper-level jet stream (ULJS) that is another important component in a macro-scale weather system. Without exception, the ULJS between 25°N and 35°N has been accompanied by the typical dust storm over South Asia, as shown in Fig. 8. Given a dynamic condition for the southward transport of dust aerosols (Fig. 5), the axis of ULJS bent southwardly in the axial direction under the influence of a non-geostrophic wind component. Since the exit area of the ULJS was very close to the ThD, a dynamic instability condition and ULJS-driven downward momentum transport are primary drivers of the eruption of the dust storm over the ThD. In Fig. 9d-f, the significant downward and upward movements can be found on both sides of the ULJS axis. The lateral secondary circulation trigged by the ULJS further enhanced the updrafts on the south side of the TP, causing more uplifted dust aerosols to higher altitudes. The southerly airflows in front of the upper trough formulated a sufficient condition to transport the dust aerosols over South Asia to the TP across the majestic Himalayas. Furthermore, the wind speed of the ULJS axis at 200 hPa decreased rapidly from 38 m/s at 9:00 to 28 m/s at 18:00 (Fig. 9b) while a low-level jet stream (LLJS) at 600 hPa level appeared and intensified along with the downward transport of energy, which was located at the north part of the ULJS axis and south part of the TP (Fig. 9a-c). In addition, the disruption of the ULJS axis over the Indian subcontinent enhanced the inflow intensity of the LLJS, which provides the important wind field for intensifying the dust storm (Sarkar et al., 2019).

Above all, the transport of dust aerosols from South Asia across the majestic Himalayas to the TP resulted from the interaction between several macro-scale weather systems. A possible transport mechanism of dust aerosols over South Asia to the TP can be summarized as a schematic diagram as shown in Fig. 10. This study demonstrated that the eruption of dust storms over South Asia is also closely related to the strong ground wind and local thermal condition. The downward energy transport of the ULJS induced the LLJS and the south-north secondary circulation with a stronger upward movement that further uplifts the dust aerosols from the ThD to higher altitudes. Consequently, the maintenance of the LPT and SBT and the southerly wind in the front of the troughs will eventually transport the dust aerosols to the TP through two routes and even further to the downstream, resulting in considerable impacts on the atmosphere and climate over these regions.

4. Conclusion and discussion

Employing the total AOD, dust CMD and DMR, and meteorological parameters from the MERRA-2 reanalysis data, this study examined the typical dust storm erupted in South Asia on 1–4 May 2018 to better understand the potential transport to the TP. This study also evaluated the spatio-temporal distribution and evolution process of the dust event based on AERONET-based and multi-source satellite-based observations. Major results derived from this study are:

- The spatio-temporal distribution and evolution process of the dust aerosol depicted by MERRA-2 data showed a good agreement with the AERONET-based and active/passive satellite-based observations.
- Under the control of the subtropical high, the northwest cold air and higher temperature anomaly in the ThD induced the eruption of this dust storm. Given the joint effects of the ULJS, the LLJS, the upper-level trough and the subtropical high, the spatial coverage of the dust storm was extended across the IGP, Southern India, the Bengal Bay and the TP.
- By the concomitant and subsequent disruption of the ULJS the significant dynamic instability condition and downward momentum transport of the ULJS induced the typical south-north secondary circulation that forms the LLJS at 600 hPa level, resulting in enhancing the inflow intensity of the LLJS. The LLJS also formulated an important dynamic condition that transports the dust aerosols more to the farther downstream.
- The coherence between the stronger upward movement of the secondary circulation and the dust aerosol from the ThD can further cause much stronger and higher vertical uplift of the dust aerosols over South Asia, which is an important prerequisite to transport the dust aerosols over South Asia to the TP across the majestic

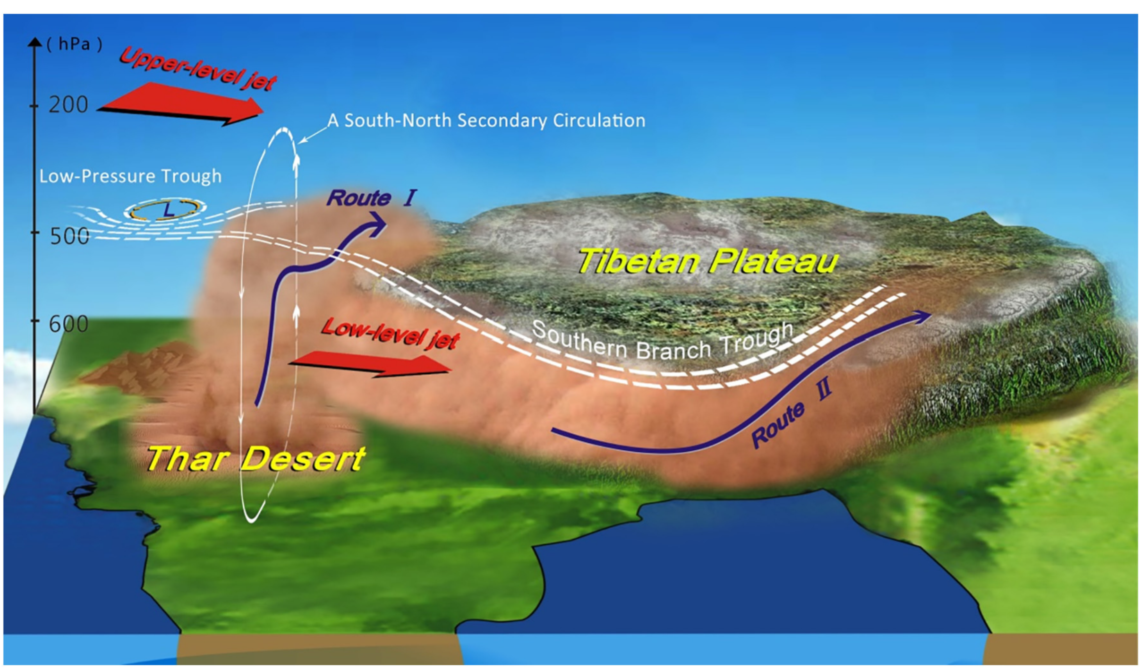

Fig. 10. A schematic diagram for the transport mechanism of dust aerosols over South Asia to the TP. The red arrows represent the ULJS at 200 hPa and LLJS at 600 hPa respectively. The white directional circle indicates the vertical secondary circulation triggered by the ULJS. The white dashed lines symbolize the atmospheric flow fields at 500 hPa level. The blue arrows represent the two transport routes to the TP. (For interpretation of the references to colour in this figure legend, the reader is referred to the web version of this article.)

Himalayas.
- The upper-level trough, i.e., a LPT over Afghanistan and a SBT trough over the Bay of Bengal, is a key dynamic factor for transporting dust aerosol to the TP. The southerly wind in the front of the upper-level trough frequently caused the uplifted dust to the TP while transport routes across the majestic Himalayas were varying with the location of the upper-level trough.

Although background air pollution levels in the TP are very low, the TP has been regularly exposed to polluted air masses along with considerable amounts of light-absorbing aerosols such as dust, smoke and atmospheric brown cloud (Ramanathan et al., 2007; Luthi et al., 2015; Wang et al., 2020a). The polluted air masses and aerosols are closely associated with the pollution emissions sourced locally and from around the TP. The northern regions of South Asia are typical sources of pollution where dust storms occur frequently during the pre-monsoon season (Satheesh et al., 2008; Das et al., 2013) and anthropogenic pollutants are heavier. Accumulated atmospheric pollution at the southern foot of the Himalayas can periodically traverse the Himalayas and reach the inland TP region through the major south-north valleys (Cong et al., 2015, Luthi et al., 2015). At the same time, the prevailing upflow across the Himalayas is driven by the large-scale westerly and small-scale southerly circulations (Zhang et al., 2020). In addition, the high-altitude cut-off low system can enhance trans-Himalaya pollution transport to the TP, which is recognized as a major pathway for long-range pollutant transport such as BC (Zhang et al., 2017a). This study systematically identified the dust transport mechanism that is the joint effects of the ULJS, the LLJS, the upper-level trough and the subtropical high over South Asia. This dust transport mechanism provides the backbone to manage natural and anthropogenic pollution to the TP. In other words, natural and anthropogenic pollutions are likely to be transported to the TP if the dynamic conditions identified in this study are formulated in South Asia. As the mechanism is derived from a dust storm case, however, further studies are necessary to comprehensively understand its importance in the trans-Himalaya pollution transport to the TP.

CRediT authorship contribution statement

Tianhe Wang: Conceptualization, Methodology, Validation, Writing - original draft, Writing - review & editing, Project administration. **Jingyi Tang:** Software, Investigation, Formal analysis, Writing - original draft, Writing - review & editing. **Mengxian Sun:** Software, Formal analysis, Investigation, Writing - original draft. **Xinwei Liu:** Formal analysis. **Yuxia Huang:** Formal analysis. **Jianping Huang:** Conceptualization, Writing - review & editing, Project administration. **Ying Han:** Software, Formal analysis. **Yifan Cheng:** Formal analysis. **Zhongwei Huang:** Formal analysis. **Jiming Li:** Formal analysis.

Declaration of competing interest

The authors declare that they have no known competing financial interests or personal relationships that could have appeared to influence the work reported in this paper.

Acknowledgments

This research is funded by the Strategic Priority Research Program, Chinese Academy of Sciences (XDA2006010301) and the National Natural Science Foundation of China (41775022, 41521004). It is also supported by NASA for making satellite datasets accessible in public. MODIS (https://ladsweb.modaps.eosdis.nasa.gov/), OMPS (https://snpp-omps.gesdisc.eosdis.nasa.gov/data/) and MERRA-2 (https://gmao.gsfc.nasa.gov/reanalysis/MERRA-2/data_access/) are managed from NASA Goddard Earth Sciences Data and Information Services Center (GES DISC). CALIPSO data is from the NASA Langley Research Center Atmospheric Science Data Center (http://eosweb.larc.nasa.gov/). We are also thankful to the efforts made by Prof. Brent Holben and other staffs in maintaining the AERONET sites and making the data available online (https://aeronet.gsfc.nasa.gov/).

Appendix A. Supplementary data

Supplementary data to this article can be found online at https://doi.org/10.1016/j.scitotenv.2020.143714.

References

Bucci, S., et al., 2014. Aerosol variability and atmospheric transport in the Himalayan region from CALIOP 2007-2010 observations. Atmos. Chem. Phys. 14, 4369–4381. https://doi.org/10.5194/acp-14-4369-2014.

Buchard, V., et al., 2017. The MERRA-2 aerosol reanalysis, 1980 onward. Part II: evaluation and case studies. J. Clim. 30, 6851–6872. https://doi.org/10.1175/Jcli-D-16-0613.1.

Cesana, G., et al., 2016. Using in situ airborne measurements to evaluate three cloud phase products derived from CALIPSO. J. Geophys. Res.-Atmos. 121, 5788–5808. https://doi.org/10.1002/2015jd024334.

Che, H., et al., 2019a. Spatial distribution of aerosol microphysical and optical properties and direct radiative effect from the China Aerosol Remote Sensing Network. Atmos. Chem. Phys. 19, 11843–11864. https://doi.org/10.5194/acp-19-11843-2019.

Che, H.Z., et al., 2019b. Large contribution of meteorological factors to inter-decadal changes in regional aerosol optical depth. Atmos. Chem. Phys. 19, 10497–10523. https://doi.org/10.5194/acp-19-10497-2019.

Cong, Z.Y., et al., 2015. Penetration of biomass-burning emissions from South Asia through the Himalayas: new insights from atmospheric organic acids. Sci. Rep. 5, 2045–2322. https://doi.org/10.1038/srep09580.

Das, S., et al., 2013. Examining mineral dust transport over the Indian subcontinent using the regional climate model, RegCM4.1. Atmos. Res. 134, 64–76. https://doi.org/10.1016/j.atmosres.2013.07.019.

Dong, L.L., et al., 2019. Linkage between moisture transport over the Yangtze River Basin and a critical area of the Tibetan Plateau during the Meiyu. Clim. Dyn. 53, 2643–2662. https://doi.org/10.1007/s00382-019-04648-w.

Flynn, L.E., et al., 2006. The ozone mapping and profiler suite. In: Qu, J.J., et al. (Eds.), Earth Science Satellite Remote Sensing. Springer, Berlin, pp. 279–296 https://doi.org/10.1007/978-3- 540-37293-6.

Flynn, L.E., et al., 2009. Measurements and products from the Solar Backscatter Ultraviolet (SBUV/2) and Ozone Mapping and Profiler Suite (OMPS) instruments. Int. J. Remote Sens. 30, 4259–4272. https://doi.org/10.1080/01431160902825040.

Gautam, R., et al., 2009. Enhanced pre-monsoon warming over the Himalayan-Gangetic region from 1979 to 2007. Geophys. Res. Lett. 36. https://doi.org/10.1029/2009gl037641.

Gelaro, R., et al., 2017. The Modern-Era Retrospective Analysis for Research and Applications, Version 2 (MERRA-2). J. Clim. 30, 5419–5454. https://doi.org/10.1175/jcli-d-16-0758.1.

Ginoux, P., et al., 2012. Global-scale attribution of anthropogenic and natural dust sources and their emission rates based on MODIS Deep Blue aerosol products. Rev. Geophys. 50, RG3005. https://doi.org/10.1029/2012rg000388.

Gul, C., et al., 2018. Concentrations and source regions of light-absorbing particles in snow/ice in northern Pakistan and their impact on snow albedo. Atmos. Chem. Phys. 18, 4981–5000. https://doi.org/10.5194/acp-18-4981-2018.

Harrison, T.C., Washington, R., Engelstaedter, S., 2019. A 14-year climatology of Saharan dust emission mechanisms inferred from automatically tracked plumes. J. Geophys. Res.-Atmos. 124, 9665–9690. https://doi.org/10.1029/2019jd030291.

Holben, B.N., et al., 1998. AERONET - a federated instrument network and data archive for aerosol characterization. Remote Sens. Environ. 66, 1–16. https://doi.org/10.1016/s0034-4257(98)00031-5.

Hsu, N.C., et al., 2013. Enhanced Deep Blue aerosol retrieval algorithm: the second generation. Journal of Geophysical Research: Atmospheres 118, 9296–9315. https://doi.org/10.1002/jgrd.50712.

Hu, Z., et al., 2020. Modeling dust sources, transport, and radiative effects at different altitudes over the Tibetan Plateau. Atmos. Chem. Phys. 20, 1507–1529. https://doi.org/10.5194/acp-20-1507-2020.

Huang, J.P., et al., 2006. Satellite-based assessment of possible dust aerosols semi-direct effect on cloud water path over East Asia. Geophys. Res. Lett. 33, L19802. https://doi.org/10.1029/2006gl026561.

Huang, J.P., et al., 2007. Summer dust aerosols detected from CALIPSO over the Tibetan Plateau. Geophys. Res. Lett. 34, L18805. https://doi.org/10.1029/2007gl029938.

Huang, J., et al., 2008. Long-range transport and vertical structure of Asian dust from CALIPSO and surface measurements during PACDEX. J. Geophys. Res. 113. https://doi.org/10.1029/2008jd010620.

Huang, J., Guan, X., Ji, F., 2012. Enhanced cold-season warming in semi-arid regions. Atmos. Chem. Phys. 12, 5391–5398. https://doi.org/10.5194/acp-12-5391-2012.

Huang, J., et al., 2014. Climate effects of dust aerosols over East Asian arid and semiarid regions. J. Geophys. Res.-Atmos. 119, 11398–11416. https://doi.org/10.1002/2014jd021796.

Huang, Z., et al., 2015. Short-cut transport path for Asian dust directly to the Arctic: a case study. Environ. Res. Lett. 10. https://doi.org/10.1088/1748-9326/10/11/114018.

Huang, Z., et al., 2018. Real-time observations of dust-cloud interactions based on polarization and Raman lidar measurements. Remote Sens. 10. https://doi.org/10.3390/rs10071017.

Huang, Z., et al., 2020. Investigation of aerosol absorption with dual-polarization lidar observations. Optical Express 28, 7028–7035. https://doi.org/10.1364/OE.390475.

Kang, S., et al., 2019. Linking atmospheric pollution to cryospheric change in the Third Pole region: current progress and future prospects. Natl. Sci. Rev. 6, 796–809. https://doi.org/10.1093/nsr/nwz031.

Kaskaoutis, D.G., et al., 2018. Impact of atmospheric circulation types on southwest Asian dust and Indian summer monsoon rainfall. Atmos. Res. 201, 189–205. https://doi.org/10.1016/j.atmosres.2017.11.002.

Kattel, D.B., Yao, T., 2018. Temperature-topographic elevation relationship for high mountain terrain: an example from the southeastern Tibetan Plateau. Int. J. Climatol. 38, E901–E920. https://doi.org/10.1002/joc.5418.

Lau, K.M., Kim, M.K., Kim, K.M., 2006. Asian summer monsoon anomalies induced by aerosol direct forcing: the role of the Tibetan Plateau. Clim. Dyn. 26, 855–864. https://doi.org/10.1007/s00382-006-0114-z.

Levy, R.C., et al., 2013. The Collection 6 MODIS aerosol products over land and ocean. Atmospheric Measurement Techniques 6, 2989–3034. https://doi.org/10.5194/amt-6-2989-2013.

Li, C., et al., 2016a. Sources of black carbon to the Himalayan-Tibetan Plateau glaciers. Nat. Commun. 7, 12574. https://doi.org/10.1038/ncomms12574.

Li, C., et al., 2016b. Concentrations and light absorption characteristics of carbonaceous aerosol in PM2.5 and PM10 of Lhasa city, the Tibetan Plateau. Atmos. Environ. 127, 340–346. https://doi.org/10.1016/j.atmosenv.2015.12.059.

Li, X., et al., 2017. Light-absorbing impurities accelerate glacier melt in the Central Tibetan Plateau. Sci. Total Environ. 587, 482–490. https://doi.org/10.1016/j.scitotenv.2017.02.169.

Liu, Z., et al., 2008. Airborne dust distributions over the Tibetan Plateau and surrounding areas derived from the first year of CALIPSO lidar observations. Atmos. Chem. Phys. 8, 5045–5060. https://doi.org/10.5194/acp-8-5045-2008.

Luthi, Z.L., et al., 2015. Atmospheric brown clouds reach the Tibetan Plateau by crossing the Himalayas. Atmos. Chem. Phys. 15, 6007–6021. https://doi.org/10.5194/acp-15-6007-2015.

Ma, X., et al., 2020. Ten-year global particulate mass concentration derived from spaceborne CALIPSO lidar observations. Sci. Total Environ. 721. https://doi.org/10.1016/j.scitotenv.2020.137699.

Mao, R., et al., 2019. The source contributions to the dust over the Tibetan Plateau: a modelling analysis. Atmos. Environ. 214. https://doi.org/10.1016/j.atmosenv.2019.116859.

Meehl, G.A., Arblaster, J.M., Collins, W.D., 2008. Effects of black carbon aerosols on the Indian monsoon. J. Clim. 21, 2869–2882. https://doi.org/10.1175/2007jcli1777.1.

Ming, J., et al., 2009. Black carbon (BC) in the snow of glaciers in west China and its potential effects on albedos. Atmos. Res. 92, 114–123. https://doi.org/10.1016/j.atmosres.2008.09.007.

Nair, V.S., et al., 2013. Black carbon aerosols over the Himalayas: direct and surface albedo forcing. Tellus Series B-Chemical and Physical Meteorology 65. https://doi.org/10.3402/tellusb.v65i0.19738.

Pandey, S.K., et al., 2017. Declining pre-monsoon dust loading over South Asia: signature of a changing regional climate. Sci. Rep. 7. https://doi.org/10.1038/s41598-017-16338-w.

Ramanathan, V., et al., 2007. Warming trends in Asia amplified by brown cloud solar absorption. Nature 448, 575–U575. https://doi.org/10.1038/nature06019.

Randles, C.A., et al., 2017. The MERRA-2 aerosol reanalysis, 1980 onward. Part I: system description and data assimilation evaluation. J. Clim. 30, 6823–6850. https://doi.org/10.1175/Jcli-D-16-0609.1.

Sarkar, S., et al., 2019. Impact of deadly dust storms (May 2018) on air quality, meteorological, and atmospheric parameters over the northern parts of India. Geohealth 3, 67–80. https://doi.org/10.1029/2018gh000170.

Satheesh, S.K., et al., 2008. Climate implications of large warming by elevated aerosol over India. Geophys. Res. Lett. 35, 6. https://doi.org/10.1029/2008gl034944.

Savtchenko, A., et al., 2004. Terra and aqua MODIS products available from NASA GES DAAC. Trace Constituents in the Troposphere and Lower Stratosphere 34, 710–714. https://doi.org/10.1016/j.asr.2004.03.012.

Sekiguchi, M., et al., 2003. A study of the direct and indirect effects of aerosols using global satellite data sets of aerosol and cloud parameters. J. Geophys. Res.-Atmos. 108. https://doi.org/10.1029/2002jd003359.

Sun, H., Liu, X., Pan, Z., 2017. Direct radiative effects of dust aerosols emitted from the Tibetan Plateau on the East Asian summer monsoon - a regional climate model simulation. Atmos. Chem. Phys. 17, 13731–13745. https://doi.org/10.5194/acp-17-13731-2017.

Thompson, A.J., et al., 2019. Modulation of mid-Holocene African rainfall by dust aerosol direct and indirect effects. Geophys. Res. Lett. 46, 3917–3926. https://doi.org/10.1029/2018gl081225.

Tiwari, S., et al., 2019. Assessment of two intense dust storm characteristics over Indo - Gangetic basin and their radiative impacts: a case study. Atmos. Res. 228, 23–40. https://doi.org/10.1016/j.atmosres.2019.05.011.

Vinoj, V., et al., 2014. Short-term modulation of Indian summer monsoon rainfall by West Asian dust. Nat. Geosci. 7, 308–313. https://doi.org/10.1038/ngeo2107.

Wang, T., et al., 2020a. Assessment of dominating aerosol properties and their long-term trend in the Pan-Third Pole region: a study with 10-year multi-sensor measurements. Atmos. Environ. 239, 117738. https://doi.org/10.1016/j.atmosenv.2020.117738.

Wang, T., et al., 2020b. Climatology of dust-forced radiative heating over the Tibetan Plateau and its surroundings. Journal of Geophysical Research: Atmospheres 125, e2020JD032942. https://doi.org/10.1029/2020JD032942.

Winker, D.M., et al., 2009. Overview of the CALIPSO mission and CALIOP data processing algorithms. J. Atmos. Ocean. Technol. 26, 2310–2323. https://doi.org/10.1175/2009jtecha1281.1.

Xu, C., et al., 2018. Tibetan Plateau impacts on global dust transport in the upper troposphere. J. Clim. 31, 4745–4756. https://doi.org/10.1175/jcli-d-17-0313.1.

Yan, H., Wang, T., 2020. Ten years of aerosol effects on single-layer overcast clouds over the US Southern Great Plains and the China Loess Plateau. Adv. Meteorol. 2020, 6719560. https://doi.org/10.1155/2020/6719160.

Yang, H., et al., 2019. Quantitative analysis of water vapor transport during Mei-Yu Front rainstorm period over the Tibetan Plateau and Yangtze-Huai River Basin. Adv. Meteorol. 2019, 14. https://doi.org/10.1155/2019/6029027.

Yao, T.D., et al., 2019. Recent third pole's rapid warming accompanies cryospheric melt and water cycle intensification and interactions between monsoon and environment: multidisciplinary approach with observations, modeling, and analysis. Bull. Am. Meteorol. Soc. 100, 423–444. https://doi.org/10.1175/Bams-D-17-0057.1.

Zhang, R.X., et al., 2017a. Enhanced trans-Himalaya pollution transport to the Tibetan Plateau by cut-off low systems. Atmos. Chem. Phys. 17, 3083–3095. https://doi.org/10.5194/acp-17-3083-2017.

Zhang, Y.L., et al., 2017b. Light-absorbing impurities enhance glacier albedo reduction in the southeastern Tibetan plateau. J. Geophys. Res.-Atmos. 122, 6915–6933. https://doi.org/10.1002/2016jd026397.

Zhang, M.X., et al., 2020. Impact of topography on black carbon transport to the southern Tibetan Plateau during the pre-monsoon season and its climatic implication. Atmos. Chem. Phys. 20, 5923–5943. https://doi.org/10.5194/acp-20-5923-2020.